Probing the inner winds of oxygen-rich evolved stars with ALMA observations of mm-wavelength SiO masers

B. Pimpanuwat*[1], A. M. S. Richards[1], M. D. Gray[1,2], S. Etoka[1], L. Decin[3] and *ATOMIUM* consortium

[1]JBCA, the University of Manchester, UK; [2]National Astronomical Research Institute of Thailand, TH; [3]KU Leuven, BE

Introduction

SiO masers found within the extended stellar atmospheres are useful for probing the inner regions of circumstellar envelopes (CSE) of evolved stars, where convection and pulsation shocks are damped and dust formation commences.

The ATOMIUM (ALMA Tracing the Origins of Molecules In dUst-forming oxygen-rich M-type stars) Large Programme[1],[2] (PI: L. Decin) observed 17 O-rich AGB and RSG stars covering a range of (circum)stellar parameters in these late stages of stellar evolution. The focus of this study is on the high-rotational quantum number (i.e. high-J) SiO masers observed in the ATOMIUM sample.

Here we highlight a few interesting results from:

ALMA Band 6 observations of high-J SiO masers around AGB stars

❖ Distributions of maser components, tracing inner winds e.g.
- Streamers   - Infalls   - Velocity gradients
❖ Focus on π^1 Gru and R Hya
❖ Investigation of mass-loss rates vs flux-weighted mean radii of fitted maser components in the ATOMIUM data set

Observations

ATOMIUM data:

❖ Frequency range 213.83-269.71 GHz, observed between 2018-2020.
❖ Mid (0".2, sensitive to thermal emission) and high (0".02, comparable to 2-4 AU for the closer targets) resolutions; low resolution (i.e. compact configuration) data not suitable for maser studies.
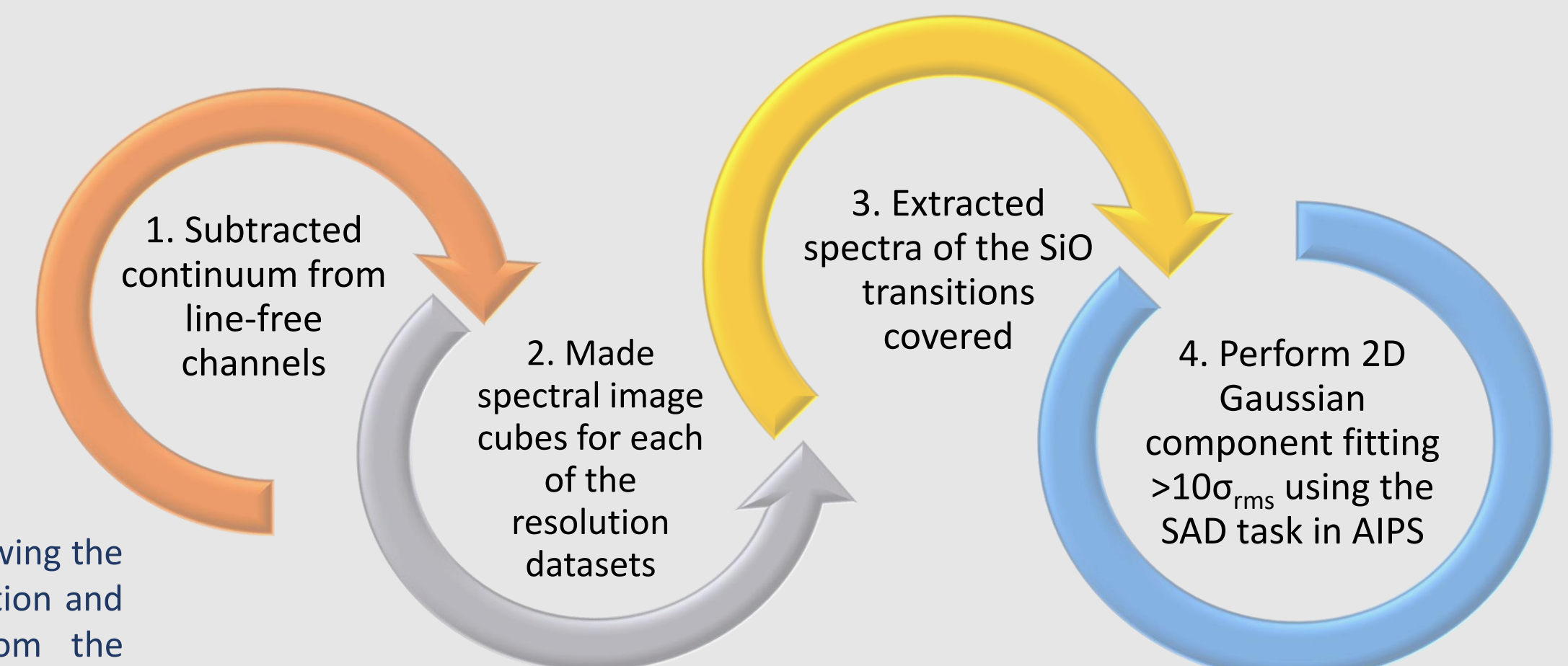❖ Contain 291 transitions of 24 different molecules[3], including 14 high-frequency (J=5-4 and 6-5) SiO lines.

Figure 1. Diagram showing the process of data reduction and analysis. Adapted from the description provided in [2].

1. Subtracted continuum from line-free channels
2. Made spectral image cubes for each of the resolution datasets
3. Extracted spectra of the SiO transitions covered
4. Perform 2D Gaussian component fitting >10σ_{rms} using the SAD task in AIPS

Results and discussions

In general:

❖ High-J maser structure: more complex than the well-studied 43 (J=1-0) and 86 (J=2-1) GHz lines, often seen in rings.
❖ The masers form clumps of typical size $\sim R_*$ and are mostly distributed between $\sim$2-4 R_*.

Notable examples:

❖ Streamers: usually show up as lines or (bipolar) cones of fitted maser components starting at or close to the stellar surface and extending radially up to $\sim$3–5 R_* (Fig. 2)
❖ Infalls: red-shifted masers detected in front of the star after max. expansion of CSE (Fig. 3)
❖ Velocity gradients: gradual change in line-of-sight velocity, typically seen in an arc. May be a sign of rotation? (Fig. 3)

A full essay on the maser component distributions will be reported in Pimpanuwat et al., *in prep.*

π^1 Gru:

❖ Shows a curved trail of entirely blue-shifted components towards the companion (black arrow in Fig. 4a).
❖ With the fitted v=0 lines, we can infer the flow pattern of the wind material subjected to the conditions caused by binary interaction; evidence of a spiral[4].
❖ Components with speeds close to the V_*; suggests tangential beaming due to an accelerating outflow caused by stellar pulsations[5].

R Hya:

❖ ^{28}SiO (and its isotopologues) v=1 J=5-4 and J=6-5: most extreme projected speeds along the NE-SW axis of position angle (PA) about 70º (dashed line in Fig. 4b).
❖ This PA agrees with the projected semi-major axis of the equatorial density enhancement (EDE) deduced from CO, suggesting a compact differentially rotating disk in the inner CSE[6].
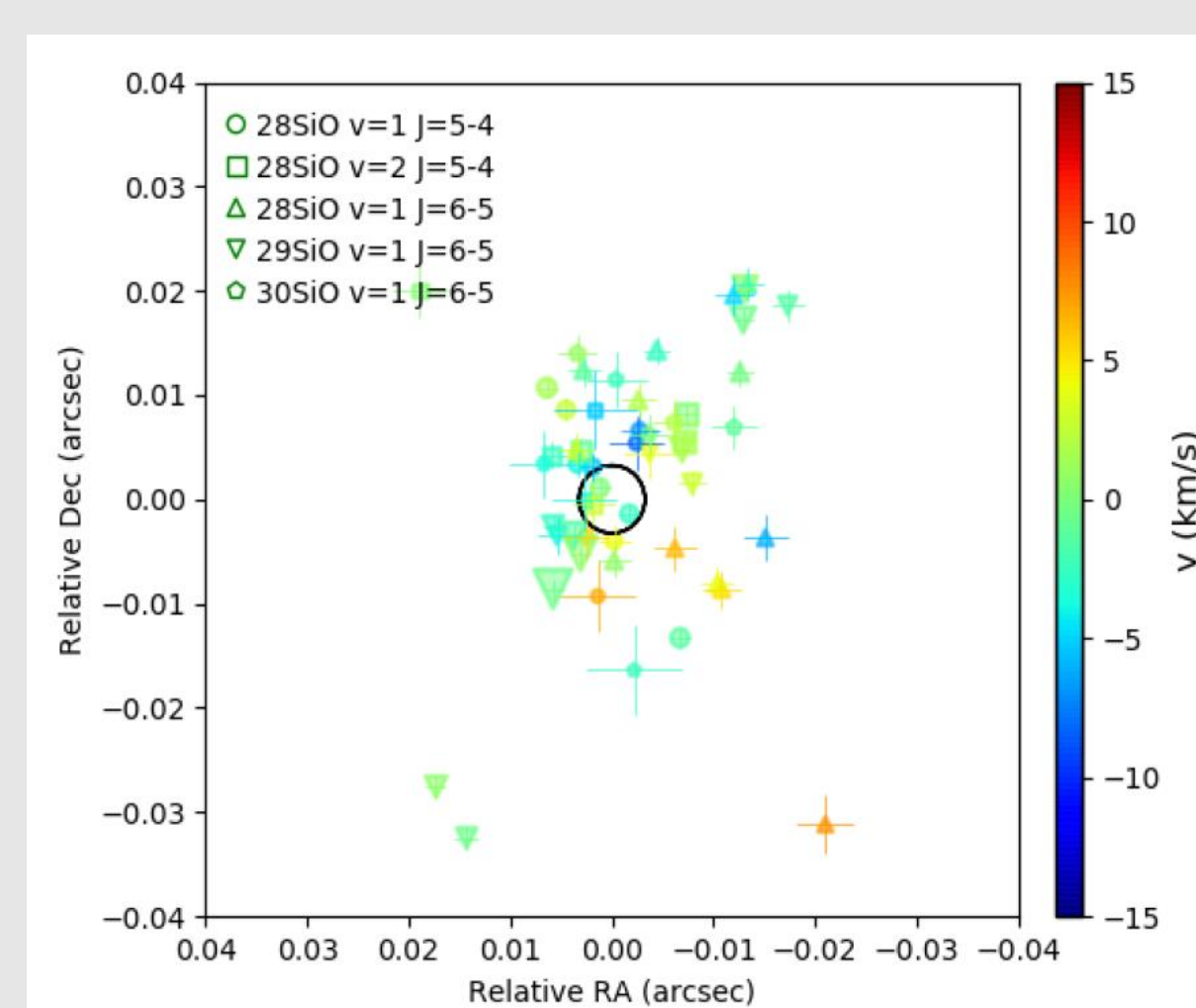

Figure 2. Position and velocity (with respect to V_*) of the SiO fitted components obtained with SAD for IRC-10529. The SiO transitions and their symbols are listed in the top left corner. The size of the symbols represents log(integrated flux), and the black circle shows the photospheric diameter of 6.5 mas. The origin is defined as the position of the source obtained from the image cubes.
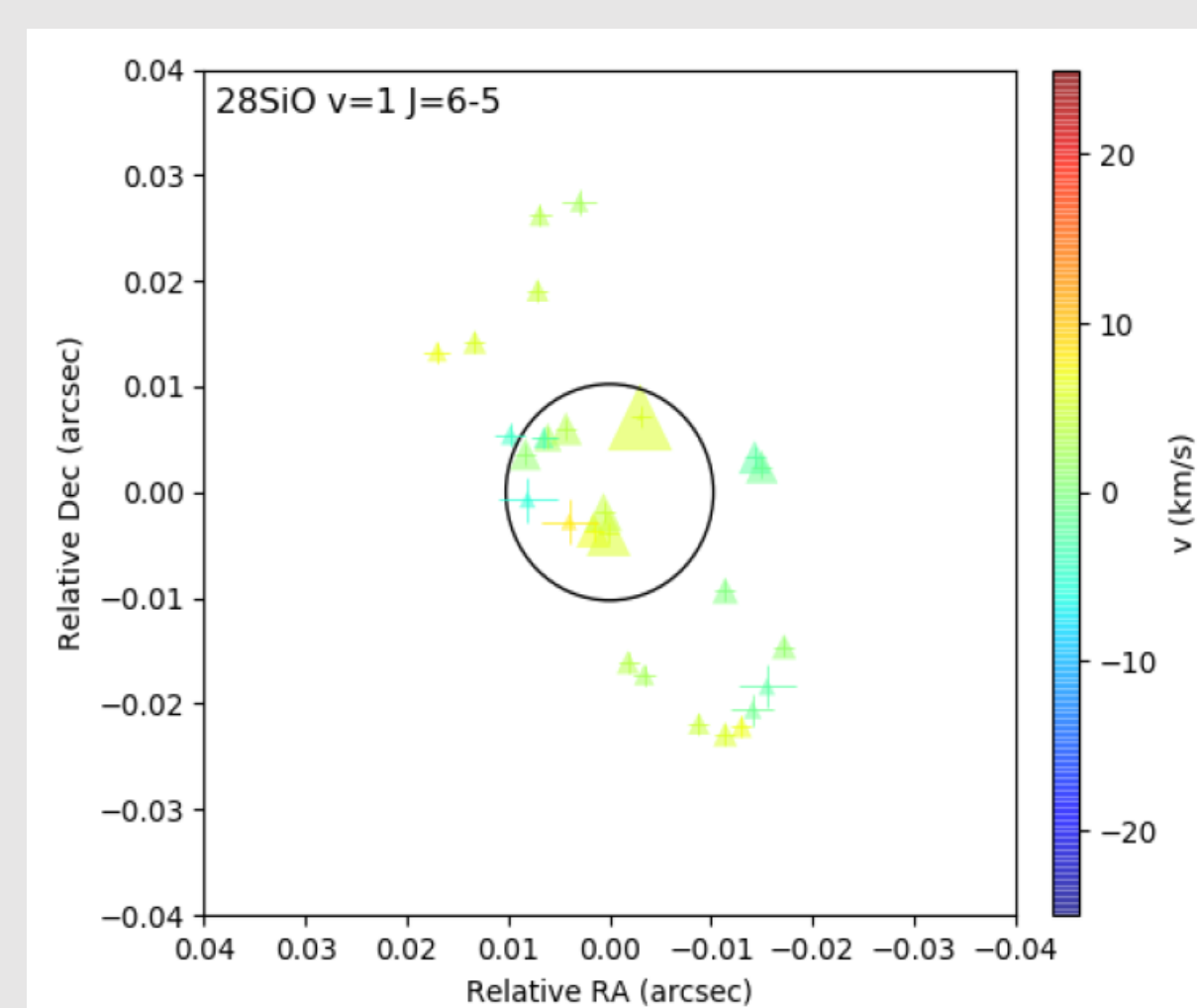

Figure 3. Similar to Fig. 2 but for the ^{28}SiO v=1 J=6-5 line towards GY Aql. The photospheric angular diameter is 21.0 mas.
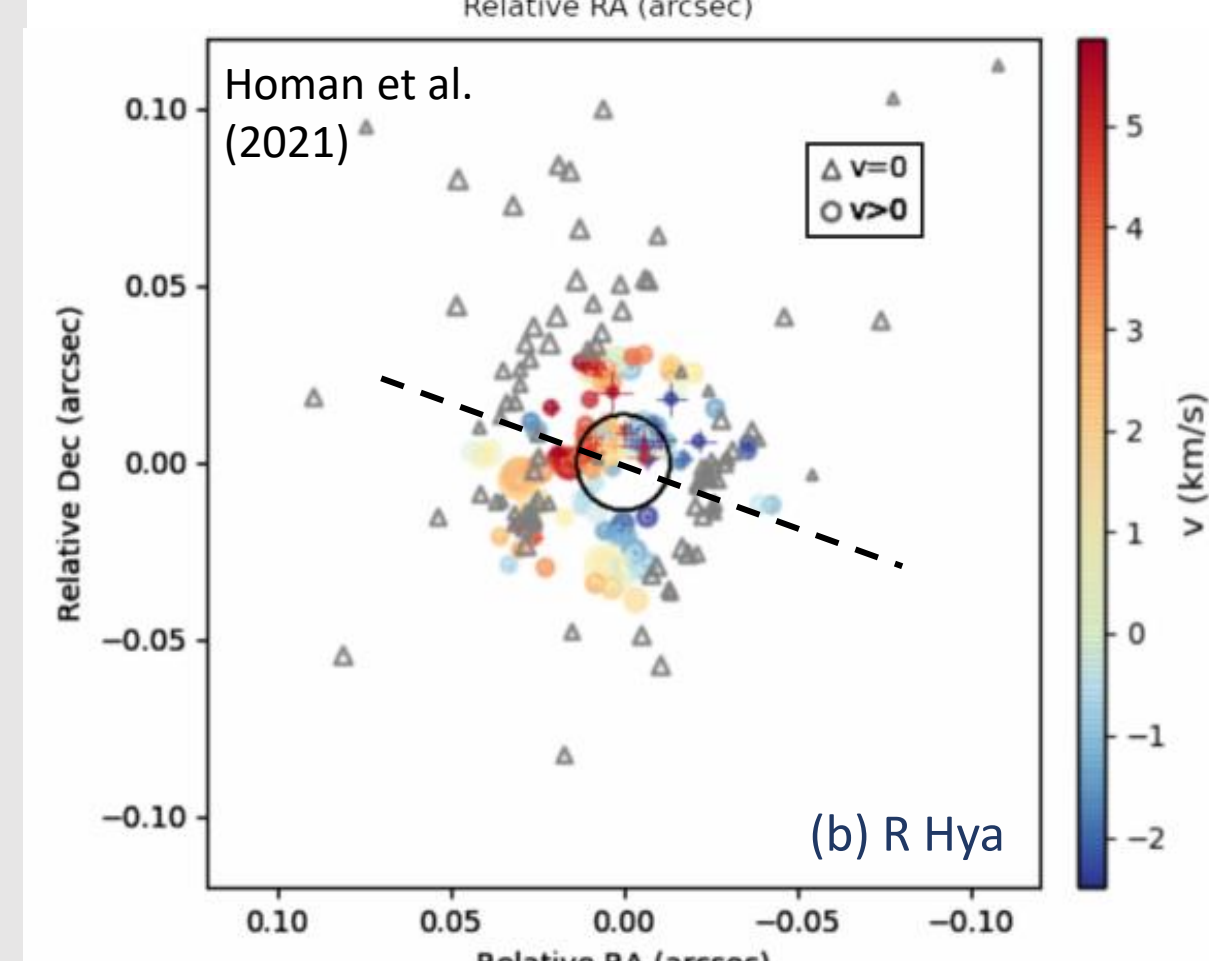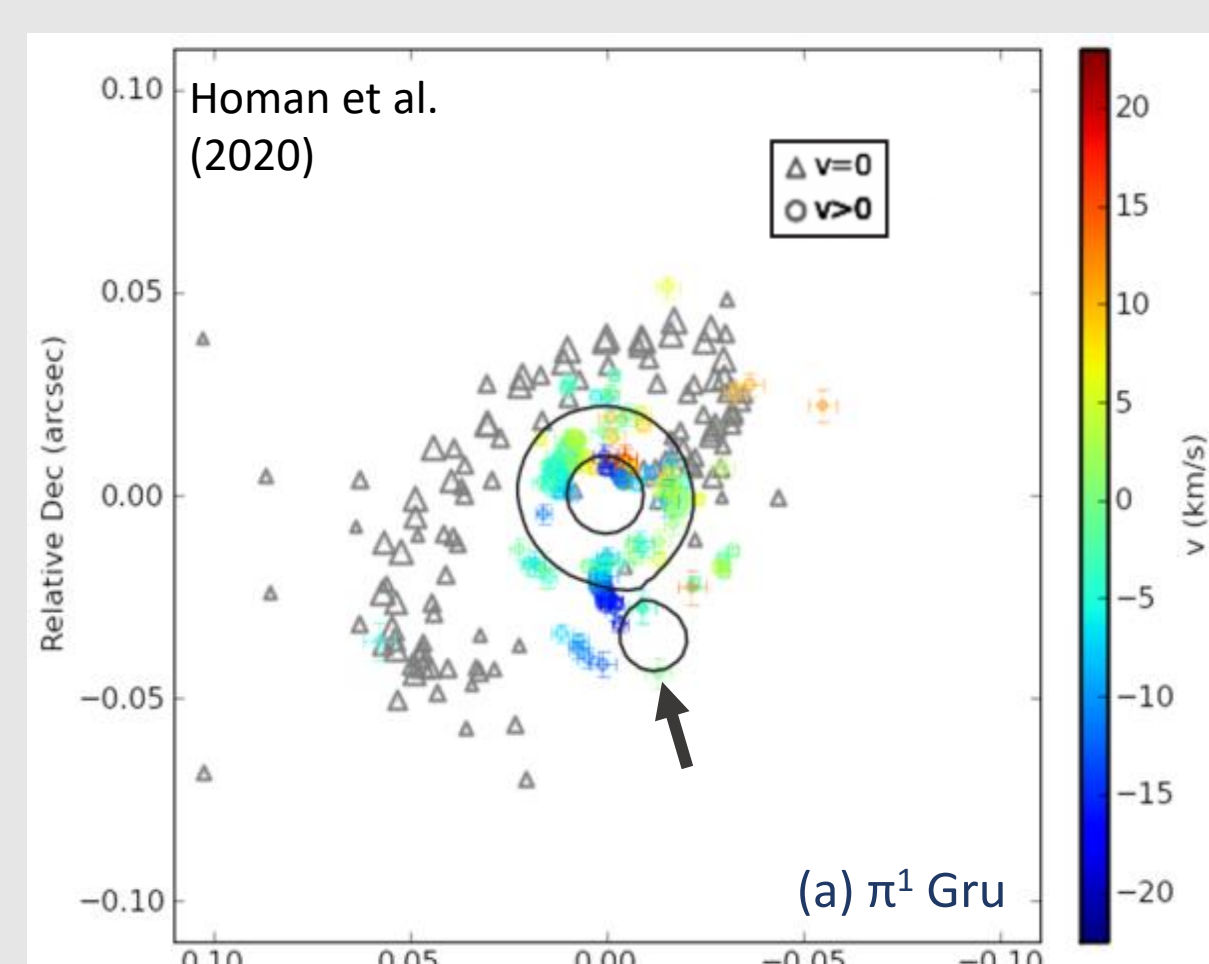

Figure 4. Position and velocity of the Gaussian-fitted components of the SiO v=1,2 J=5-4 and J=6-5 emission lines of the high-resolution dataset observed towards π^1 Gru (a) and R Hya (b). For π^1 Gru, contours of the 120 and 768 times the continuum rms noise value (1.5×10^{-5} Jy/beam) are shown while the black circle in (b) represents the stellar photosphere of R Hya. The marker size scales as log$_{10}$ of the integrated flux and the velocities are given relative to the V_*. The grey triangles mark the positions of the mid-resolution components of v=0 transitions. Note the different colour bars used in the plots.

Mass-loss rate *vs* mean size of maser shell

❖ The flux-weighted mean radius of the fitted maser components for each maser source is defined as the angular distance from the star in which 90% of the total emission is enclosed[7].
❖ Plotted against the mass-loss rate of its respective star (Fig. 5).
❖ Suggest **strong correlation in v=1 J=6-5 (0.85), v=1 J=5-4 (0.50) and v=2 J=5-4 (0.71)** transitions.
❖ Need to determine the flux-weighted radius in 3D as many bright maser components lie close to or in front of the star in the line-of-sight direction.
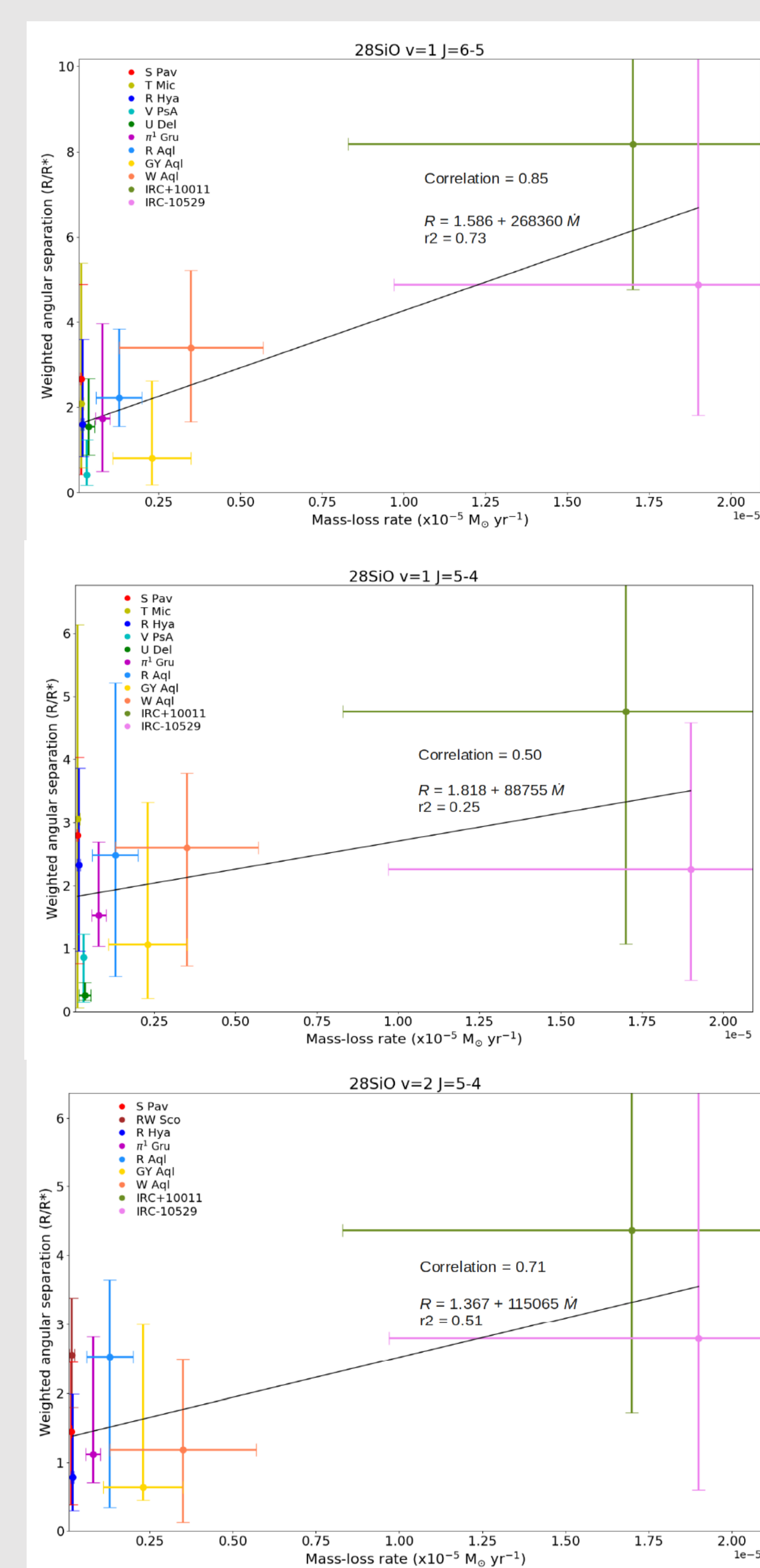❖ May also be intrinsic to the nature of the maser transitions. Further analysis is necessary.

Figure 5. Plots of flux-weighted angular distance of fitted maser components against mass-loss rate for ^{28}SiO v=1 J=6-5 (*top*), v=1 J=5-4 (*middle*), and v=2 J=5-4 (*bottom*). The correlation coefficients and the best-fitted linear regression models, along with its coefficient of determination (r2), are given and plotted (black solid line) for the three transitions.

Only the AGB sources with > 10 components were selected as the sample.

Summary

❖ Some of the recent results of the analysis of J=5-4 and 6-5 SiO masers, observed between Autumn 2018 and Spring 2020 by ALMA, are presented and discussed.

❖ Mass-loss rates and flux-weighted mean radii of SiO components appear correlated, but the exclusion of the line-of-sight direction means a more robust study is required before drawing any conclusions.

References

[1] Decin et al. 2020, *Science*, 368, 6510, pp1497-1500.
[2] Gottlieb et al. 2022, *A&A*, 660, A94.
[3] Wallström et al. 2023, *A&A,* accepted.
[4] Homan et al., 2020, *A&A*, 644, A61.
[5] Chapman, J. M. & Cohen, R. J. 1985, *MNRAS*, 212, 375.
[6] Homan et al. 2021, *A&A*, 651, A82.
[7] Assaf, K.A., Diamond, P.J., Richards, A.M.S., Gray, M.D., 2011, *MNRAS*, 415, 2, pp1083-1092

*Contact - bpimpanuwat@gmail.com